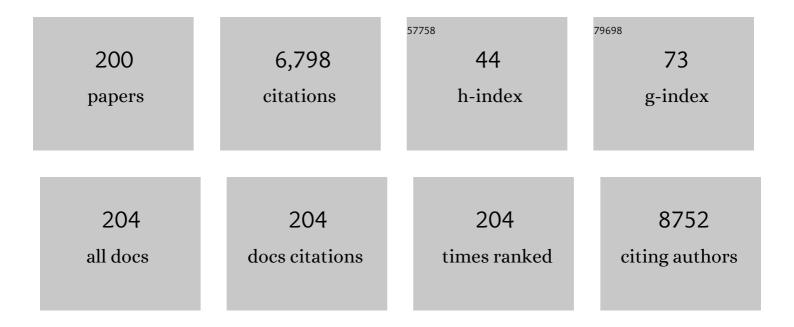
## List of Publications by Year in descending order

Source: https://exaly.com/author-pdf/1192406/publications.pdf Version: 2024-02-01



FENC CAO

#	Article	IF	CITATIONS
1	Electronic and Morphological Dual Modulation of Cobalt Carbonate Hydroxides by Mn Doping toward Highly Efficient and Stable Bifunctional Electrocatalysts for Overall Water Splitting. Journal of the American Chemical Society, 2017, 139, 8320-8328.	13.7	745
2	DNA interactions of a functionalized ruthenium(II) mixed-polypyridyl complex [Ru(bpy)2ppd]2+. Journal of Inorganic Biochemistry, 2006, 100, 1487-1494.	3.5	247
3	NiFe <sub>2</sub> O <sub>4</sub> Nanoparticles/NiFe Layered Double-Hydroxide Nanosheet Heterostructure Array for Efficient Overall Water Splitting at Large Current Densities. ACS Applied Materials & Interfaces, 2018, 10, 26283-26292.	8.0	219
4	An Fe-doped nickel selenide nanorod/nanosheet hierarchical array for efficient overall water splitting. Journal of Materials Chemistry A, 2019, 7, 2233-2241.	10.3	215
5	Mxene/carbon nanohorn/β-cyclodextrin-Metal-organic frameworks as high-performance electrochemical sensing platform for sensitive detection of carbendazim pesticide. Journal of Hazardous Materials, 2020, 396, 122776.	12.4	204
6	Fabrication of defect-rich MoS <sub>2</sub> ultrathin nanosheets for application in lithium-ion batteries and supercapacitors. Journal of Materials Chemistry A, 2015, 3, 19445-19454.	10.3	175
7	Versatile Threeâ€Dimensional Porous Cu@Cu <sub>2</sub> O Aerogel Networks as Electrocatalysts and Mimicking Peroxidases. Angewandte Chemie - International Edition, 2018, 57, 6819-6824.	13.8	168
8	A Co-doped Ni–Fe mixed oxide mesoporous nanosheet array with low overpotential and high stability towards overall water splitting. Journal of Materials Chemistry A, 2018, 6, 167-178.	10.3	158
9	Fluorescent blood glucose monitor by hemin-functionalized graphene quantum dots based sensing system. Analytica Chimica Acta, 2014, 810, 71-78.	5.4	127
10	Stress Effects on Meat Quality: A Mechanistic Perspective. Comprehensive Reviews in Food Science and Food Safety, 2019, 18, 380-401.	11.7	126
11	Replacement strategies for non-green dipolar aprotic solvents. Green Chemistry, 2020, 22, 6240-6257.	9.0	102
12	Control of hybrid AC/DC microgrid under islanding operational conditions. Journal of Modern Power Systems and Clean Energy, 2014, 2, 223-232.	5.4	100
13	MXene@Ag-based ratiometric electrochemical sensing strategy for effective detection of carbendazim in vegetable samples. Food Chemistry, 2021, 360, 130006.	8.2	100
14	Dithiocarbamate-modified starch derivatives with high heavy metal adsorption performance. Carbohydrate Polymers, 2016, 136, 30-37.	10.2	98
15	Kinetically Controlled Coprecipitation for General Fast Synthesis of Sandwiched Metal Hydroxide Nanosheets/Graphene Composites toward Efficient Water Splitting. Advanced Functional Materials, 2018, 28, 1704594.	14.9	91
16	Allâ€polymer solar cells with over 16% efficiency and enhanced stability enabled by compatible solvent and polymer additives. Aggregate, 2022, 3, e58.	9.9	85
17	Nanozyme-Modified Metal–Organic Frameworks with Multienzymes Activity as Biomimetic Catalysts and Electrocatalytic Interfaces. ACS Applied Materials & Interfaces, 2020, 12, 17185-17192.	8.0	81
18	Magnetic Fe 3 O 4 nanoparticles induced effects on performance and microbial community of activated sludge from a sequencing batch reactor under long-term exposure. Bioresource Technology, 2017, 225, 377-385.	9.6	80

#	Article	IF	CITATIONS
19	Degradation of bisphenol A through transition metals activating persulfate process. Ecotoxicology and Environmental Safety, 2018, 158, 239-247.	6.0	79
20	Sequential Functionalization of <i>meta</i> -C–H and <i>ipso</i> -C–O Bonds of Phenols. Journal of the American Chemical Society, 2019, 141, 1903-1907.	13.7	79
21	Targeting topoisomerase II with the chiral DNA-intercalating ruthenium(II) polypyridyl complexes. Journal of Biological Inorganic Chemistry, 2007, 12, 1015-1027.	2.6	78
22	Two-Photon Semiconducting Polymer Dots with Dual-Emission for Ratiometric Fluorescent Sensing and Bioimaging of Tyrosinase Activity. Analytical Chemistry, 2016, 88, 7372-7377.	6.5	77
23	Ratiometric detection of copper ions and alkaline phosphatase activity based on semiconducting polymer dots assembled with rhodamine B hydrazide. Biosensors and Bioelectronics, 2017, 91, 70-75.	10.1	72
24	Synthesis, GC selective DNA binding and topoisomerase II inhibition activities of ruthenium(II) polypyridyl complex containing 11-aminopteridino[6,7-f][1,10]phenanthrolin-13(12H)-one. Journal of Inorganic Biochemistry, 2008, 102, 1050-1059.	3.5	70
25	Colorimetric and Phosphorimetric Dual-Signaling Strategy Mediated by Inner Filter Effect for Highly Sensitive Assay of Organophosphorus Pesticides. Journal of Agricultural and Food Chemistry, 2015, 63, 8947-8954.	5.2	69
26	Bright up-conversion green photoluminescence in Ho3+-Yb3+ co-doped Bi4Ti3O12 ferroelectric thin films. Journal of Applied Physics, 2011, 109, .	2.5	62
27	Performance and microbial community of a sequencing batch biofilm reactor treating synthetic mariculture wastewater under long-term exposure to norfloxacin. Bioresource Technology, 2016, 222, 139-147.	9.6	62
28	Carbon nanodots–chitosan composite film: A platform for protein immobilization, direct electrochemistry and bioelectrocatalysis. Biosensors and Bioelectronics, 2014, 58, 351-358.	10.1	60
29	Magnetic amine-functionalized polyacrylic acid-nanomagnetite for hexavalent chromium removal from polluted water. RSC Advances, 2015, 5, 60208-60219.	3.6	57
30	DNA Binding, Photocleavage, and Topoisomerase Inhibition of Functionalized Ruthenium(II)â€Polypyridine Complexes. Chemistry and Biodiversity, 2008, 5, 1962-1979.	2.1	56
31	NiO@Ni-MOF nanoarrays modified Ti mesh as ultrasensitive electrochemical sensing platform for luteolin detection. Talanta, 2020, 215, 120891.	5.5	55
32	Artificial nanozyme based on platinum nanoparticles anchored metal-organic frameworks with enhanced electrocatalytic activity for detection of telomeres activity. Biosensors and Bioelectronics, 2020, 149, 111838.	10.1	54
33	Performance evaluation, microbial enzymatic activity and microbial community of a sequencing batch reactor under long-term exposure to cerium dioxide nanoparticles. Bioresource Technology, 2016, 220, 262-270.	9.6	53
34	The evidence of porcine hemagglutinating encephalomyelitis virus induced nonsuppurative encephalitis as the cause of death in piglets. PeerJ, 2016, 4, e2443.	2.0	52
35	In Vitro Transcription Inhibition by Ruthenium(II) Polypyridyl Complexes with Electropositive Ancillary Ligands. Inorganic Chemistry, 2009, 48, 5599-5601.	4.0	50
36	Herpes Simplex Virus 1 Infection of Tree Shrews Differs from That of Mice in the Severity of Acute Infection and Viral Transcription in the Peripheral Nervous System. Journal of Virology, 2016, 90, 790-804.	3.4	49

#	Article	IF	CITATIONS
37	A Family of Neutral-Point-Clamped Circuits of Single-Phase PV Inverters: Generalized Principle and Implementation. IEEE Transactions on Power Electronics, 2017, 32, 4307-4319.	7.9	49
38	A Mitochondria-Targeted Ratiometric Biosensor for pH Monitoring and Imaging in Living Cells with Congo-Red-Functionalized Dual-Emission Semiconducting Polymer Dots. Analytical Chemistry, 2017, 89, 11703-11710.	6.5	48
39	Operation and Modulation of H7 Current-Source Inverter With Hybrid SiC and Si Semiconductor Switches. IEEE Journal of Emerging and Selected Topics in Power Electronics, 2018, 6, 387-399.	5.4	48
40	pH responsive "off–on–off―luminescent switch of a novel ruthenium(II) complex [Ru(bpy)2(pipipH2)]2+. Inorganic Chemistry Communication, 2007, 10, 170-173.	3.9	47
41	Global Synchronous Pulse Width Modulation of Distributed Inverters. IEEE Transactions on Power Electronics, 2016, 31, 6237-6253.	7.9	47
42	Strong upconversion luminescence properties of Yb3+ and Er3+ codoped Bi4Ti3O12 ferroelectric thin films. Journal of Applied Physics, 2009, 106, 126104.	2.5	46
43	A Voltage Detection Method for the Voltage Ride-Through Operation of Renewable Energy Generation Systems Under Grid Voltage Distortion Conditions. IEEE Transactions on Sustainable Energy, 2015, 6, 1131-1139.	8.8	45
44	A Closed-Loop Time-Domain Analysis Method for Modular Multilevel Converter. IEEE Transactions on Power Electronics, 2017, 32, 7494-7508.	7.9	45
45	Covalent Surface Functionalization of Semiconducting Polymer Dots with β-Cyclodextrin for Fluorescent Ratiometric Assay of Cholesterol through Host–Guest Inclusion and FRET. Langmuir, 2016, 32, 12725-12731.	3.5	43
46	Porcine Hemagglutinating Encephalomyelitis Virus Activation of the Integrin α5β1-FAK-Cofilin Pathway Causes Cytoskeletal Rearrangement To Promote Its Invasion of N2a Cells. Journal of Virology, 2019, 93,	3.4	42
47	Methanol/Oxygen Enzymatic Biofuel Cell Using Laccase and NAD <sup>+</sup> -Dependent Dehydrogenase Cascades as Biocatalysts on Carbon Nanodots Electrodes. ACS Applied Materials & Interfaces, 2017, 9, 40978-40986.	8.0	39
48	Interfacial electronic modulation of CoP-CoO p-p type heterojunction for enhancing oxygen evolution reaction. Journal of Colloid and Interface Science, 2022, 607, 1343-1352.	9.4	39
49	Long-term effects of cupric oxide nanoparticles (CuO NPs) on the performance, microbial community and enzymatic activity of activated sludge in a sequencing batch reactor. Journal of Environmental Management, 2017, 187, 330-339.	7.8	38
50	Porcine Hemagglutinating Encephalomyelitis Virus Enters Neuro-2a Cells via Clathrin-Mediated Endocytosis in a Rab5-, Cholesterol-, and pH-Dependent Manner. Journal of Virology, 2017, 91, .	3.4	38
51	Versatile Threeâ€Dimensional Porous Cu@Cu <sub>2</sub> O Aerogel Networks as Electrocatalysts and Mimicking Peroxidases. Angewandte Chemie, 2018, 130, 6935-6940.	2.0	36
52	Two-Photon Fluorescent Nanoprobe for Glutathione Sensing and Imaging in Living Cells and Zebrafish Using a Semiconducting Polymer Dots Hybrid with Dopamine and β-Cyclodextrin. Analytical Chemistry, 2019, 91, 12414-12421.	6.5	36
53	Novel electrochemical sensing platform based on a molecularly imprinted polymer-decorated 3D-multi-walled carbon nanotube intercalated graphene aerogel for selective and sensitive detection of dopamine. Analytical Methods, 2020, 12, 1845-1851.	2.7	34
54	Effect of ancillary ligands on the topoisomerases II and transcription inhibition activity of polypyridyl ruthenium(II) complexes. Journal of Inorganic Biochemistry, 2010, 104, 576-582.	3.5	33

#	Article	IF	CITATIONS
55	Bright up-conversion photoluminescence of Bi4â^' <i>x</i> Er <i>x</i> Ti3O12 ferroelectric thin films. Journal of Applied Physics, 2011, 109, 043106-043106-5.	2.5	33
56	Further analyses on the phylogeny of the subclass Scuticociliatia (Protozoa, Ciliophora) based on both nuclear and mitochondrial data. Molecular Phylogenetics and Evolution, 2019, 139, 106565.	2.7	33
57	Synthesis, crystal structure and DNA-binding properties of ruthenium(II) polypyridyl complexes with dicationic 2,2′-dipyridyl derivatives as ligands. Polyhedron, 2008, 27, 2845-2850.	2.2	32
58	"Turn-On―Fluorescence Determination of β-Glucosidase Activity Using Fluorescent Polymer Nanoparticles Formed from Polyethylenimine Cross-Linked with Hydroquinone. ACS Applied Polymer Materials, 2019, 1, 3057-3063.	4.4	32
59	Cyclometalated Iridium(III) Complexes as High-Sensitivity Two-Photon Excited Mitochondria Dyes and Near-Infrared Photodynamic Therapy Agents. Inorganic Chemistry, 2020, 59, 14920-14931.	4.0	32
60	Effects of salinity on pollutant removal and bacterial community in a partially saturated vertical flow constructed wetland. Bioresource Technology, 2021, 329, 124890.	9.6	32
61	Spectroscopy, NMR and DFT studies on molecular recognition of crown ether bridged chiral heterotrinuclear salen Zn(II) complex. Spectrochimica Acta - Part A: Molecular and Biomolecular Spectroscopy, 2005, 62, 886-895.	3.9	30
62	Control of Parallel-Connected Modular Multilevel Converters. IEEE Transactions on Power Electronics, 2015, 30, 372-386.	7.9	28
63	Protein Localization Analysis of Essential Genes in Prokaryotes. Scientific Reports, 2014, 4, 6001.	3.3	27
64	Synthesis of High-Quality Multilayer Hexagonal Boron Nitride Films on Au Foils for Ultrahigh Rejection Ratio Solar-Blind Photodetection. ACS Applied Materials & Interfaces, 2020, 12, 28351-28359.	8.0	27
65	Preparation of quaternized chitosan/Ag composite nanogels in inverse miniemulsions for durable and antimicrobial cotton fabrics. Carbohydrate Polymers, 2022, 278, 118935.	10.2	27
66	pH responsive luminescent switches of ruthenium(II) complexes containing two imidazole groups: Synthesis, spectroscopy, electrochemistry and theoretical calculations. Inorganica Chimica Acta, 2009, 362, 4960-4966.	2.4	26
67	Strong Upconversion Photoluminescence and Large Ferroelectric Polarization in Er <sup>3+</sup> –Yb <sup>3+</sup> –W <sup>6+</sup> Triply Substituted Bismuth Titanate Thin Films Prepared by Chemical Solution Deposition. Journal of the American Ceramic Society, 2011, 94, 3867-3870.	3.8	26
68	A new EV71 VP3 epitope in norovirus P particle vector displays neutralizing activity and protection in vivo in mice. Vaccine, 2015, 33, 6596-6603.	3.8	26
69	Induction of Atypical Autophagy by Porcine Hemagglutinating Encephalomyelitis Virus Contributes to Viral Replication. Frontiers in Cellular and Infection Microbiology, 2017, 7, 56.	3.9	25
70	Synthesis, DNAâ€Binding and Photocleavage Studies of the Ruthenium(II) Complexes [Ru(phen) <sub>2</sub> (ppd)] <sup>2+</sup> and [Ru(phen)(ppd) <sub>2</sub> ] <sup>2+</sup> (ppd=Pteridino[6,7â€ <i>f</i> ] [1,10]phenanthrolineâ€1,13(10 <i>H</i> ,12 <i>H</i> )â€dione,) Tj ETQq0 0	0 rgBT /O	verlock 10 Tf
71	Effect of florfenicol on performance and microbial community of a sequencing batch biofilm reactor treating mariculture wastewater. Environmental Technology (United Kingdom), 2018, 39, 363-372.	2.2	24
72	Au Nanocrystals@Defective Amorphous MnO <sub>2</sub> Nanosheets Core/Shell Nanostructure with Effective CO <sub>2</sub> Adsorption and Activation toward CO <sub>2</sub> Electroreduction	6.7	24

with Effective CO<sub>2</sub> Adsorption and Activation toward CO<sub>2</sub> Electroreduction to CO. ACS Sustainable Chemistry and Engineering, 2021, 9, 5230-5239. 72 6.7

#	Article	IF	CITATIONS
73	Synonymous codon usage analysis of hand, foot and mouth disease viruses: A comparative study on coxsackievirus A6, A10, A16, and enterovirus 71 from 2008 to 2015. Infection, Genetics and Evolution, 2017, 53, 212-217.	2.3	23
74	Long-term effects of nickel oxide nanoparticles on performance, microbial enzymatic activity, and microbial community of a sequencing batch reactor. Chemosphere, 2017, 169, 387-395.	8.2	23
75	Utility of 7,8-dihydroxyflavone in preventing astrocytic and synaptic deficits in the hippocampus elicited by PTSD. Pharmacological Research, 2022, 176, 106079.	7.1	23
76	Reactivation of HSV-1 following explant of tree shrew brain. Journal of NeuroVirology, 2016, 22, 293-306.	2.1	22
77	A Dual-Input Central Capacitor DC/DC Converter for Distributed Photovoltaic Architectures. IEEE Transactions on Industry Applications, 2017, 53, 305-318.	4.9	22
78	2DÂleaf-like ZIF-L decorated with multi-walled carbon nanotubes as electrochemical sensing platform for sensitively detecting thiabendazole pesticide residues in fruit samples. Analytical and Bioanalytical Chemistry, 2021, 413, 7485-7494.	3.7	22
79	Synthesis, Characterization, and DNA-Binding Properties of the Chiral Ruthenium(II) Complexes Δ- and ĥ-[Ru(bpy)2(dmppd)]2+ (dmppd = 10,12-Dimethylpteridino[6,7-f] [1,10]phenanthroline-11,13(1	0H, <b>12</b> H)-di	ion <b>e;)</b> Tj ETQic
80	General Strategy to Achieve Color-Tunable Ratiometric Two-Photon Integrated Single Semiconducting Polymer Dot for Imaging Hypochlorous Acid. ACS Nano, 2021, 15, 13633-13645.	14.6	21
81	Effects of intercalative ligands on the DNA binding, DNA topoisomerase II and DNA transcription inhibition of polypyridyl ruthenium(II) complexes. Inorganica Chimica Acta, 2011, 378, 140-147.	2.4	20
82	StructureActivity Relationship of Polypyridyl Ruthenium(II) Complexes as DNA Intercalators, DNA Photocleavage Reagents, and DNA Topoisomerase and RNA Polymerase Inhibitors. Chemistry and Biodiversity, 2013, 10, 367-384.	2.1	20
83	Two-Layer Global Synchronous Pulse Width Modulation Method for Attenuating Circulating Leakage Current in PV Station. IEEE Transactions on Industrial Electronics, 2018, 65, 8005-8017.	7.9	20
84	A Carrier Synchronization Method for Global Synchronous Pulsewidth Modulation Application Using Phase-Locked Loop. IEEE Transactions on Power Electronics, 2019, 34, 10720-10732.	7.9	20
85	Paclitaxel Induces Sex-biased Behavioral Deficits and Changes in Gene Expression in Mouse Prefrontal Cortex. Neuroscience, 2020, 426, 168-178.	2.3	20
86	miR-142-5p Disrupts Neuronal Morphogenesis Underlying Porcine Hemagglutinating Encephalomyelitis Virus Infection by Targeting Ulk1. Frontiers in Cellular and Infection Microbiology, 2017, 7, 155.	3.9	19
87	Ti <sub>3</sub> C <sub>2</sub> T <sub>x</sub> MXene/nitrogen-doped reduced graphene oxide composite: a high-performance electrochemical sensing platform for adrenaline detection. Nanotechnology, 2021, 32, 265501.	2.6	19
88	Ginsenoside Rg1 Prevents Cognitive Impairment and Hippocampal Neuronal Apoptosis in Experimental Vascular Dementia Mice by Promoting GPR30 Expression. Neural Plasticity, 2021, 2021, 1-11.	2.2	19
89	Synthesis, DNA-binding and photocleavage studies of cobalt(III) complexes [Co(bpy)2(dpta)]3+ and [Co(bpy)2(amtp)]3+. Transition Metal Chemistry, 2007, 32, 271-277.	1.4	18
90	Polypyridyl Complexes of Ruthenium(II): Stabilization of Gâ€quadruplex DNA and Inhibition of Telomerase Activity. ChemPlusChem, 2012, 77, 551-562.	2.8	18

#	Article	IF	CITATIONS
91	Ulk1 Governs Nerve Growth Factor/TrkA Signaling by Mediating Rab5 GTPase Activation in Porcine Hemagglutinating Encephalomyelitis Virus-Induced Neurodegenerative Disorders. Journal of Virology, 2018, 92, .	3.4	18
92	Sensitive electrochemical platform for trace determination of Pb2+ based on multilayer Bi-MOFs/reduced graphene oxide films modified electrode. Mikrochimica Acta, 2020, 187, 603.	5.0	18
93	Ultrasmall Pt Nanoparticles-Loaded Crystalline MoO <sub>2</sub> /Amorphous Ni(OH) <sub>2</sub> Hybrid Nanofilms with Enhanced Water Dissociation and Sufficient Hydrogen Spillover for Hydrogen Generation. ACS Sustainable Chemistry and Engineering, 2021, 9, 8257-8269.	6.7	18
94	Deadâ€ŧime elimination method of nineâ€switch converter. IET Power Electronics, 2014, 7, 1759-1769.	2.1	17
95	Detection of Thrombin Based on Fluorescence Energy Transfer between Semiconducting Polymer Dots and BHQ-Labelled Aptamers. Sensors, 2018, 18, 589.	3.8	17
96	A metal–organic framework with multienzyme activity as a biosensing platform for real-time electrochemical detection of nitric oxide and hydrogen peroxide. Analyst, The, 2021, 146, 2609-2616.	3.5	17
97	Technical optimization and life cycle assessment of environment-friendly superplasticizer for concrete engineering. Chemosphere, 2021, 281, 130955.	8.2	17
98	ATN-161 reduces virus proliferation in PHEV-infected mice by inhibiting the integrin α5β1-FAK signaling pathway. Veterinary Microbiology, 2019, 233, 147-153.	1.9	16
99	Sensitive determination of nitrite by using an electrode modified with hierarchical three-dimensional tungsten disulfide and reduced graphene oxide aerogel. Mikrochimica Acta, 2019, 186, 291.	5.0	16
100	Morphogenetic characters of the model ciliate Euplotes vannus (Ciliophora, Spirotrichea): Notes on cortical pattern formation during conjugational and postconjugational reorganization. European Journal of Protistology, 2020, 73, 125675.	1.5	16
101	Boosting the sensitivity of pH responsible luminescent switches of polypyridyl ruthenium(II) complexes by structural design. Inorganic Chemistry Communication, 2012, 16, 25-27.	3.9	15
102	Identification of the Replication Origins from Cyanothece ATCC 51142 and Their Interactions with the DnaA Protein: From In Silico to In Vitro Studies. Frontiers in Microbiology, 2015, 6, 1370.	3.5	15
103	Communication-less harmonic compensation in a multi-bus microgrid through autonomous control of distributed generation grid-interfacing converters. Journal of Modern Power Systems and Clean Energy, 2015, 3, 597-609.	5.4	15
104	The PERK/PKR-eIF2α Pathway Negatively Regulates Porcine Hemagglutinating Encephalomyelitis Virus Replication by Attenuating Global Protein Translation and Facilitating Stress Granule Formation. Journal of Virology, 2022, 96, JVI0169521.	3.4	15
105	Reconfigurable self-powered imaging photodetectors by reassembling and disassembling ZnO/perovskite heterojunctions. Journal of Materials Chemistry C, 2022, 10, 8922-8930.	5.5	15
106	Eukaryote-like Ser/Thr protein kinase PrkA modulates sporulation via regulating the transcriptional factor σK in Bacillus subtilis. Frontiers in Microbiology, 2015, 06, 382.	3.5	14
107	Organic semiconductor polymer nanodots as a new kind of off-on fluorescent probe for sulfide. Mikrochimica Acta, 2017, 184, 445-451.	5.0	14
108	Single-crystalline titanium dioxide hollow tetragonal nanocones with large exposed (1 0 1) facets for excellent photocatalysis. Journal of Colloid and Interface Science, 2017, 490, 420-429.	9.4	14

#	Article	IF	CITATIONS
109	Self-template synthesis of flower-like hierarchical graphene/copper oxide@copper(II) metal-organic framework composite for the voltammetric determination of caffeic acid. Mikrochimica Acta, 2020, 187, 258.	5.0	14
110	A photostable reaction-based A–A–A type two-photon fluorescent probe for rapid detection and imaging of sulfur dioxide. Journal of Materials Chemistry B, 2021, 9, 3554-3562.	5.8	14
111	Depichering the Effects of Astragaloside IV on AD-Like Phenotypes: A Systematic and Experimental Investigation. Oxidative Medicine and Cellular Longevity, 2021, 2021, 1-21.	4.0	14
112	Dual-Emission Carbonized Polymer Dots for Ratiometric pH Sensing, pH-Dependent Generation of Singlet Oxygen, and Imaging-Guided Dynamics Monitoring of Photodynamic Therapy. ACS Applied Bio Materials, 2021, 4, 7663-7672.	4.6	14
113	Quantitative evaluation of the non-thermal effect in microwave induced polymer curing. RSC Advances, 2021, 11, 3740-3750.	3.6	14
114	Prussian blue-carboxylated MWCNTs/ZIF-67 composite: a new electrochemical sensing platform for paracetamol detection with high sensitivity. Nanotechnology, 2021, 32, 085501.	2.6	14
115	Dual-Targeting into the Mitochondria of Cancer Cells for Ratiometric Investigation of the Dynamic Fluctuation of Sulfur Dioxide and Formaldehyde with Two-Photon Integrated Semiconducting Polymer Dots. ACS Applied Materials & Interfaces, 2022, 14, 179-190.	8.0	14
116	Gene-expression patterns in the cerebral cortex of mice infected with porcine haemagglutinating encephalomyelitis virus detected using microarray. Journal of General Virology, 2014, 95, 2192-2203.	2.9	13
117	Effect of magnesium oxide nanoparticles on microbial diversity and removal performance of sequencing batch reactor. Journal of Environmental Management, 2018, 222, 475-482.	7.8	13
118	Genomic characterization of two Orf virus isolates from Jilin province in China. Virus Genes, 2019, 55, 490-501.	1.6	13
119	MiR-10a-5p-Mediated Syndecan 1 Suppression Restricts Porcine Hemagglutinating Encephalomyelitis Virus Replication. Frontiers in Microbiology, 2020, 11, 105.	3.5	13
120	Orf Virus ORF120 Protein Positively Regulates the NF-κB Pathway by Interacting with G3BP1. Journal of Virology, 2021, 95, e0015321.	3.4	13
121	Light-activated semiconducting polymer dots as mimic oxidases with remarkable catalytic efficiency: characteristics, mechanisms, and applications. Chemical Communications, 2020, 56, 3035-3038.	4.1	13
122	Chitosan assisted synthesis of 3D graphene@Au nanosheet composites: catalytic reduction of 4-nitrophenol. RSC Advances, 2015, 5, 79456-79462.	3.6	12
123	miR-21a-5p Contributes to Porcine Hemagglutinating Encephalomyelitis Virus Proliferation via Targeting CASK-Interactive Protein1 In vivo and vitro. Frontiers in Microbiology, 2017, 8, 304.	3.5	12
124	Novel polypyridyl ruthenium complexes acting as high affinity DNA intercalators, potent transcription inhibitors and antitumor reagents. Journal of Inorganic Biochemistry, 2018, 185, 1-9.	3.5	12
125	Ratiometric Sensing for Alkaline Phosphatase Based on Two Independent Signals from in Situ Formed Nanohybrids of Semiconducting Polymer Nanoparticles and MnO <sub>2</sub> Nanosheets. ACS Omega, 2019, 4, 8282-8289.	3.5	12
126	Br-Doped CuO Multilamellar Mesoporous Nanosheets with Oxygen Vacancies and Cetyltrimethyl Ammonium Cations Adsorption for Optimizing Intermediate Species and Their Adsorption Behaviors toward CO <sub>2</sub> Electroreduction to Ethanol with a High Faradaic Efficiency. Inorganic Chemistry, 2021, 60, 14371-14381.	4.0	12

#	Article	IF	CITATIONS
127	Selective Binding and Reverse Transcription Inhibition of Single-Strand poly(A) RNA by Metal TMPyP Complexes. Inorganic Chemistry, 2014, 53, 10015-10017.	4.0	11
128	Graphene oxide-stimulated acoustic attenuating performance of tungsten based epoxy films. Journal of Materials Chemistry C, 2015, 3, 10848-10855.	5.5	11
129	Fast Symmetrical Component Extraction From Unbalanced Three-Phase Signals Using Non-Nominal <i>dq </i> -Transformation. IEEE Transactions on Power Electronics, 2018, 33, 9134-9141.	7.9	11
130	Operational Analyses and Control Scheme of Nine-Arm Modular Multilevel Converter. IEEE Transactions on Power Electronics, 2020, 35, 3416-3433.	7.9	11
131	MSNs-Based Nanocomposite for Biofilm Imaging and NIR-Activated Chem/Photothermal/Photodynamic Combination Therapy. ACS Applied Bio Materials, 2021, 4, 2810-2820.	4.6	11
132	Synthesis, characterization and hydrogen storage capacity of MS2 (M = Mo, Ti) nanotubes. Frontiers of Chemistry in China: Selected Publications From Chinese Universities, 2006, 1, 260-263.	0.4	10
133	Synthesis, DNA-binding and DNA-photocleavage properties of ruthenium(II) mixed-polypyridyl complex [Ru(tbz)2(dppz)]2+. Journal of Molecular Structure, 2008, 892, 485-489.	3.6	10
134	Semiconducting-polymer-dot based fluorescent probe for turn-on sensing of phytic acid. Analytical Methods, 2016, 8, 7755-7761.	2.7	10
135	Control strategy of MMC battery energy storage system under asymmetrical grid voltage condition. Chinese Journal of Electrical Engineering, 2016, 2, 76-83.	3.4	10
136	Genomic characterization and pathogenicity of a porcine hemagglutinating encephalomyelitis virus strain isolated in China. Virus Genes, 2018, 54, 672-683.	1.6	10
137	Insights into long-term effects of amino-functionalized multi-walled carbon nanotubes (MWCNTs-NH2) on the performance, enzymatic activity and microbial community of sequencing batch reactor. Environmental Pollution, 2019, 254, 113118.	7.5	10
138	An Experimental Model of Neurodegenerative Disease Based on Porcine Hemagglutinating Encephalomyelitis Virus–Related Lysosomal Abnormalities. Molecular Neurobiology, 2020, 57, 5299-5306.	4.0	10
139	Performance evaluation and microbial community shift of a sequencing batch reactor under silica nanoparticles stress. Bioresource Technology, 2017, 245, 673-680.	9.6	9
140	Preparation of thermoresponsive poly( <i>N</i> â€vinylcaprolactamâ€ <i>coâ€</i> 2â€methoxyethyl acrylate) nanogels via inverse miniemulsion polymerization. Journal of Applied Polymer Science, 2019, 136, 48237.	2.6	9
141	Replacing halogenated solvents by a butyl acetate solution of bisphenol S in the transformations of indoles. Green Chemistry, 2021, 23, 3588-3594.	9.0	9
142	Synthesis, Characterization, and DNA Binding Studies of Ruthenium(II) Complexes with 2-Pyridyl-1H-anthra[1,2-d]imidazole-6,11-dione. Australian Journal of Chemistry, 2008, 61, 732.	0.9	8
143	Further analyses on the evolutionary "keyâ€protist― <i>Halteria</i> (Protista, Ciliophora) based on transcriptomic data. Zoologica Scripta, 2019, 48, 813-825.	1.7	8
144	A near-infrared upconversion luminescence total internal reflection platform for quantitative image analysis. Chemical Communications, 2020, 56, 8440-8443.	4.1	8

#	Article	IF	CITATIONS
145	Synthesis of carboxy-cyclobutane isomers combining an amide bond and self-assembly of coordination polymers in the solid state: controlling the reaction site of [2 + 2] cycloaddition by introducing a substituent group. Inorganic Chemistry Frontiers, 2021, 8, 1997-2007.	6.0	8
146	Petrogenesis and tectonic setting of the early-middle triassic subduction-related granite in the eastern segment of East Kunlun: evidences from petrology, geochemistry, and zircon U-Pb-Hf isotopes. International Geology Review, 2022, 64, 698-721.	2.1	8
147	The mechanism of the plant roots' soil-reinforcement based on generalized equivalent confining pressure. PeerJ, 2020, 8, e10064.	2.0	8
148	pH-Responsive Fluorescent Polymer–Drug System for Real-Time Detection and <i>In Situ</i> Eradication of Bacterial Biofilms. ACS Biomaterials Science and Engineering, 2022, 8, 893-902.	5.2	8
149	The matrix protein of vesicular stomatitis virus inhibits host-directed transcription of target genes via interaction with the TFIIH subunit p8. Veterinary Microbiology, 2017, 208, 82-88.	1.9	7
150	Dipolar HCP materials as alternatives to DMF solvent for azide-based synthesis. Green Chemistry, 2021, 23, 7499-7505.	9.0	7
151	The vertical heterogeneity of soil detachment by overland flow on the waterâ€level fluctuation zone slope in the Three Gorges Reservoir, China. Hydrological Processes, 2021, 35, e14282.	2.6	7
152	The Change Characteristics of Potential Habitat and Fishing Season for Neon Flying Squid in the Northwest Pacific Ocean under Future Climate Change Scenarios. Marine and Coastal Fisheries, 2021, 13, 450-462.	1.4	7
153	Core–shell Cu@C@ZIF-8 composite: a high-performance electrode material for electrochemical sensing of nitrite with high selectivity and sensitivity. Nanotechnology, 2022, 33, 225501.	2.6	7
154	Performance enhancement of a self-powered imaging CsPbBr <sub>3</sub> photodetector by tuning the trap effects of carriers. Journal of Materials Chemistry C, 2022, 10, 7460-7468.	5.5	7
155	Hexavalent chromium induced tunable surface functionalization of graphite. RSC Advances, 2016, 6, 58354-58362.	3.6	6
156	Sequential <i>ortho</i> -C–H and <i>ipso</i> -C–O Functionalization Using a Bifunctional Directing Group. Organic Letters, 2019, 21, 7928-7932.	4.6	6
157	Water-soluble branched polymer for combined chemo-immunotherapy of bacterial infections. Biomaterials Science, 2021, 9, 8347-8355.	5.4	6
158	Polypyridyl ruthenium complexes as bifunctional TAR RNA binders and HIV-1 reverse transcriptase inhibitors. Journal of Inorganic Biochemistry, 2022, 234, 111880.	3.5	6
159	Combination of FACS and Homologous Recombination for the Generation of Stable and High-Expression Engineered Cell Lines. PLoS ONE, 2014, 9, e91712.	2.5	5
160	Mode characteristics of silver-coated inverted-wedge silica microdisks. Science China: Physics, Mechanics and Astronomy, 2015, 58, 1.	5.1	5
161	Development of a lateral flow immunochromatographic assay for the rapid diagnosis of Orf virus infections. Journal of Virological Methods, 2016, 236, 10-17.	2.1	5
162	Role of autophagy in cellular response to infection with Orf virus Jilin isolate. Veterinary Microbiology, 2016, 193, 22-27.	1.9	5

#	Article	IF	CITATIONS
163	EIF3i affects vesicular stomatitis virus growth by interacting with matrix protein. Veterinary Microbiology, 2017, 212, 59-66.	1.9	5
164	Long-term impacts of carboxyl functionalized multi-walled carbon nanotubes on the performance, microbial enzymatic activity and microbial community of sequencing batch reactor. Bioresource Technology, 2019, 286, 121382.	9.6	5
165	Excellent catalytic properties of luminescent Cu@Cu <sub>2</sub> S nanozymes and their antibacterial applications. Chemical Communications, 2022, 58, 2995-2998.	4.1	5
166	Spectroscopic and theoretical studies on axial coordination of bis(pyrrol-2-ylmethyleneamine)phenyl complexes. Spectrochimica Acta - Part A: Molecular and Biomolecular Spectroscopy, 2008, 71, 191-198.	3.9	4
167	Navigation line detection based on robotic vision in natural vegetation-embraced environment. , 2010, , ,		4
168	Global synchronous discontinuous pulse width modulation method with fast calculation capability for distributed three-phase inverters. Journal of Modern Power Systems and Clean Energy, 2016, 4, 103-112.	5.4	4
169	miR-142a-3p promotes the proliferation of porcine hemagglutinating encephalomyelitis virus by targeting Rab3a. Archives of Virology, 2020, 165, 345-354.	2.1	4
170	Evaluating the Contribution of the Physical and Biochemical Effects of Root on Detachment for the Coarse-Textured Soil from the Three Gorges Reservoir, China. Eurasian Soil Science, 2020, 53, 1260-1269.	1.6	4
171	Porcine haemagglutinating encephalomyelitis virus deactivates transcription factor IRF3 and limits type I interferon production. Veterinary Microbiology, 2021, 252, 108918.	1.9	4
172	Porcine Hemagglutinating Encephalomyelitis Virus Triggers Neural Autophagy Independently of ULK1. Journal of Virology, 2021, 95, e0085121.	3.4	4
173	Synthesis, spectral and theoretical studies on axial coordination of dinuclear Salen zinc(II) complexes. Journal of Coordination Chemistry, 2007, 60, 2485-2497.	2.2	3
174	Prediction of yield of retail cuts for native and crossbred Chinese Yellow cattle. Animal Science Journal, 2007, 78, 440-444.	1.4	3
175	Fabrication of Fe <sub>3</sub> O <sub>4</sub> / <i>O</i> arboxylmethyl Chitosan Magnetic Particle Assembles in Inverse Miniemulsions for Loading and Release of Bovine Serum Albumin. ChemistrySelect, 2020, 5, 8344-8351.	1.5	3
176	Porcine hemagglutinating encephalomyelitis virus induces atypical autophagy via opposite regulation of expression and nuclear translocation of transcription factor EB. Veterinary Microbiology, 2021, 255, 109015.	1.9	3
177	Singlet-oxygen generated by a metal–organic framework for electrochemical biosensing. Journal of Materials Chemistry B, 2021, 9, 4670-4677.	5.8	3
178	Cell-surface glycans act as attachment factors for porcine hemagglutinating encephalomyelitis virus. Veterinary Microbiology, 2022, 265, 109315.	1.9	3
179	Evidence of Microglial Immune Response Following Coronavirus PHEV Infection of CNS. Frontiers in Immunology, 2021, 12, 804625.	4.8	3
180	Ultrasensitive electrochemical biosensor for protein detection based on target-triggering cascade enzyme-free signal amplification strategy. Analytica Chimica Acta, 2022, 1202, 339675.	5.4	3

#	Article	IF	CITATIONS
181	Easy Fabrication of Amorphous Covalent Organic Nanospheres Using Schiffâ€Base Chemistry for Iodine Capture. Chemistry - an Asian Journal, 2022, 17, .	3.3	3
182	Terpyridyl ruthenium complexes as visible spectral probe for poly(A) RNA and bifunctional TAR RNA binders and HIV-1 reverse transcriptase inhibitors. Inorganica Chimica Acta, 2022, 539, 121027.	2.4	3
183	Scorpion-Shaped Zinc Porphyrins as Tetrafunctional TAR RNA Predators and HIV-1 Reverse Transcriptase Inhibitors. Inorganic Chemistry, 2022, 61, 10774-10780.	4.0	3
184	Synthesis, characterization and cd spectra studies of chiral calixsalen complexes. Chinese Journal of Chemistry, 2001, 19, 1296-1301.	4.9	2
185	Editorial: DNA Replication Origins in Microbial Genomes. Frontiers in Microbiology, 2016, 6, 1545.	3.5	2
186	New Discovery of <i>Neocalamites</i> from the Upper Triassic Daheba Formation in West Qinling, Northwest China. Acta Geologica Sinica, 2019, 93, 756-757.	1.4	2
187	Mechanistic investigation on moistureâ€induced softening of poly(vinyl acetate)â€stiffened polyester fabrics. Journal of Applied Polymer Science, 2020, 137, 49316.	2.6	2
188	Host factor cyclophilin B affects Orf virus replication by interacting with viral ORF058 protein. Veterinary Microbiology, 2021, 258, 109099.	1.9	2
189	Kalman filter estimation of the number of competing terminals in IEEE802.11 network based on the modified Markov model. , 2010, , .		1
190	Performance of video over an IEEE 802.11a wireless LAN. , 2011, , .		1
191	Discovery of Early Paleozoic Garnet Amphibolite in the Wenquan Complex, Northern Margin of the Yili Block, NW China. Acta Geologica Sinica, 2021, 95, 696-698.	1.4	1
192	Electrochemical biosensor based on singlet oxygen generated by molecular photosensitizers. Analytica Chimica Acta, 2021, 1183, 338970.	5.4	1
193	Porphyrin decorated Cu2O nanocrystals for electroanalytical detection of S-Nitrosothiols. Analytica Chimica Acta, 2022, 1202, 339687.	5.4	1
194	Versatile metal organic frameworks as catalysis and indicator of nitric oxide. Journal of Materials Chemistry B, 2022, , .	5.8	1
195	The Optical Integrative Switching networks supporting 3G mobile communications. , 2009, , .		0
196	A Minimized Wilkinson Power Divider Using Dual Transmission Line. , 2009, , .		0
197	The Throughput Analysis of IEEE 802.11a WLAN with Low-Rate Access Nodes. , 2012, , .		0
198	UV-enhanced oxidative quenching of PFO–PFPV Pdots for ratiometric quantification and imaging of hypochlorous acid in living cells. Journal of Materials Science, 2021, 56, 17732-17746.	3.7	0

#	Article	IF	CITATIONS
199	Four-year imaging follow-up of a homozygous familial hypercholesterolaemia patient: atherosclerosis ingravescence and coronary flow velocity reserve reduced gradually. Case report. Medical Ultrasonography, 2015, 17, 401.	0.8	0
200	Microtubule depolymerization limits porcine betacoronavirus PHEV replication. Veterinary Microbiology, 2022, 269, 109448.	1.9	0